The 9th European Congress on Computational Methods in Applied Sciences and Engineering
ECCOMAS Congress 2024
3 – 7 June 2024, Lisboa, Portugal

MACHINE LEARNING MODEL FOR CORRELATING MICROSTRUCTURAL FEATURES AND MACROSCOPIC PROPERTIES OF HETEROGENEOUS COMPOSITES

CHENGCHENG SHEN[1,2], HAIFENG ZHAO[1,2,†], RUINAN MU[1,2], ANPING WANG[1,2], KE WANG[1,2]

[1]University of Chinese Academy of Sciences
[2]Key Laboratory of Space Utilization, Technology and Engineering Center for Space Utilization, Chinese Academy of Sciences
Beijing, China
[†] Corresponding email: hfzhao@csu.ac.cn

Key words: Machine learning, artificial neural network (ANN), convolutional neural network (CNN), nickel base superalloys, fibrous and particulate composites, thermal conductivity, hardness.

Summary. This study explores the use of machine learning (ML) models in predicting the macroscopic properties of heterogeneous composites. Traditional micromechanics parameters have limitations, thus ML models with and without feature engineering are utilized. For artificial neural network (ANN) models with feature engineering, microstructural descriptors from SEM images of nickel-based superalloys are used to predict hardness. 10 descriptors are selected to reduce the computational cost of the deep neural network (DNN) with the support of the shallow neural network (SNN), and accuracy is enhanced by incorporating two additional descriptors. The result surpasses existing physics-based models. Models without feature engineering employ a convolutional neural network (CNN) to predict the effective thermal conductivity of thermal insulation composite materials. The CNN model demonstrates accurate predictions for novel microstructures. ML models can achieve more efficient predictions than traditional methods, indicating their potential in advancing materials science. In summary, harnessing artificial intelligence to capture the scattering characteristics of heterogeneous materials enables both DNN and CNN models to achieve more efficient predictions compared to traditional methods. This highlights the potential of machine learning in advancing materials science and expediting the development of materials with desired properties.

1 INTRODUCTION

Composite materials with complex multi-scale microstructure typically exhibit great performance[1, 2]. At the same time, the complex multi-scale microstructure also hinders the accurate description and performance prediction of computational modeling of composite materials [3, 4]. Traditional computational models are constrained by limited input parameters, restricting their capacity to extract features from complex microstructures and effectively describe heterogeneous composites.[5]. For example, in the traditional micromechanics context,

the size and volume fraction of inclusions have long been regarded as the primary microstructural parameters dictating macroscopic properties[6-8]. Obviously, traditional models frequently struggle to achieve a comprehensive understanding of the intrinsic characteristics of materials, let alone analyze the impact of each feature on macroscopic properties.

Machine learning (ML) automates the creation of computing models using training data, rather than relying on manually coded programs with predetermined logic. [9]. Therefore, with the accumulation of material experimental data and microstructural characterization, ML methods can be used to accurately and quickly perform multi-scale calculations of materials and correlate the material microstructure and macroscopic properties[10]. It also can infer the composition[11], microstructure[12], and even preparation process parameters[13], etc. from the macroscopic properties of the material, which can provide guidance for reverse design of materials[14, 15]. The integration of ML techniques into materials research is a key focus in modern scientific investigation, inspired by AI4Science [16, 17].

Artificial neural network (ANN) is one of the commonly used machine learning models, which can establish a complex nonlinear mapping between input material description parameters and output properties[18, 19]. ANN model preparation requires feature engineering based on educated intuition, whereas CNN models take images directly as input without the need for explicit feature engineering. As one of the deep learning models, convolutional neural network (CNN) has the ability to automatically extract features from input pictures. These features may influence material macroscopic properties in ways beyond existing physical models. The CNN model receives microstructural information more comprehensively and accurately predicts the macroscopic properties of the material[20, 21].

This research includes two ML models of artificial neural network (ANN) and convolutional neural network (CNN) models. ANN models correlate microstructural data with the hardness of alloy materials[22], whereas CNN models predict the effective thermal conductivity (ETC) of thermal insulation composites using microstructure images [23]. The execution processes of the ANN and CNN models are shown in **Figure 1**. In general, the process of using ML model includes data preparation, model training, and prediction. The difference between the two models is the presence or absence of feature engineering. The raw microstructural images are obtained by experiment or numerical simulation. After feature extraction and weight ranking, the image is converted into numerical values and used as the input of the ANN. While CNN directly takes the images as input. Then the two ML models are trained and tested. The prediction results of ML models are more accurate and efficient than traditional physics-based models. Additionally, CNN model is also used to predict novel types of microstructures beyond training set.

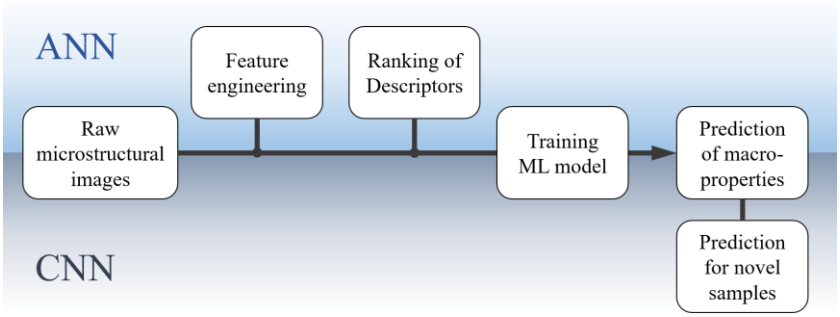

Figure 1. Workflow of machine learning models for predicting macroscopic properties of materials using microstructure information, the blue part above represents the steps for ANN, and the gray part below represents the steps for CNN.

2 MATERIAL AND DATA PREPARATION

In this section, microstructural information of a nickel-based superalloy specimen with γ′ precipitates are prepared for ANN model training. The raw SEM images and some processing parameters are transformed to numerical values by feature engineering and weight ranking[22]. The unit representative image generated by numerical simulation and the ETC value of thermal insulation composites calculated by mesoscopic simulation are used as CNN training data[23].

2.1 Microstructural image preparation

The research of correlating between hardness and microstructural data is based on an nickel-based superalloy specimen. Powder compacted specimen are prepared using the gradient cooling method, and hundreds of SEM images are generated to study different microstructures of γ′ precipitates. In **Figure 2**(a), some SEM images showcasing γ′ precipitate distribution and morphology variations linked to cooling rate, and the Vicker hardness measurement positions is corresponding to the microstructure observation position. The average precipitate sizes and their volume fraction gradually increase from the specimen bottom to the top part. The origin training data for ANN model has 483 SEM images and value of Vicker hardness at corresponding position.

For alloy materials, it is relatively convenient to conduct high-throughput hardness measurement experiments, but the cost of thermal conductivity measurements when studying insulating materials is still relatively high. Therefore, the research of mapping microstructure and macroscopic property ETC of thermal insulation composites is using the representative volume element (RVE) approach generated by numerical methods[24, 25], as shown in **Figure 2**(b). These RVEs are close to the real fibrous or particulate microstructures of thermal insulation composite materials. Then a two-dimensional nine-speed D2Q9 Lattice Boltzmann method (LBM)[26] mesoscopic simulation is used to calculate ETCs of RVEs. For ETC prediction case, one sample includes one image RVE as input, and two ETCs of *x* and *y* direction as outputs. The training set for CNN model has 4000 samples and test set has 400 samples.

(a) (b)

Figure 2. (a) SEM observations showing the gradient distribution of γ′ precipitates from the superalloy specimen; (b) Representative images of reconstructed microstructure of thermal insulation composites.

2.2 Feature engineering: extracting microstructural descriptors

As mentioned in the introduction, the CNN model uses images one by one as input, while the ANN model needs to extract feature values from the pictures as inputs.

Before extracting microstructural features, the SEM images of alloy specimen are binarized and segmented. And the γ′ precipitates are differentiated from the matrix by grayscales of image. Then 24 descriptors of microstructural are extracted by an image processing software. These descriptors are divided into two categories: dispersion state and geometry of γ′ precipitates. Another category of descriptor is alloy specimen processing parameter -- cooling rate. Totally, 3 categories including 25 descriptors are as ANN inputs, the details are shown in **Table 1**.

Table 1: The definition of microstructural descriptors and cooling rate of γ′ precipitates.

Number	Descriptor	Definition	Type
1	VF	Volume fraction	Dispersion
2	X	X Center (Pxl)	
3	Y	Y Center (Pxl)	
4	N	Number of γ' precipitation cluster	
5	D	Distance to scene border (Pxl)	
6	SD_a	Standard deviation of area	Geometry
7	A	Area (Pxl)	
8	SI	Shape index, $SI = P/4\sqrt{A}$	
9	δ_{cmp}	Compactness [32]	
10	L_b	Border length	
11	θ_m	Main direction, $\theta_m = \arctan(l_{mly}/l_{mlx})$, l_{mly}/l_{mlx}means the inclination of main line	
12	δ_{rnd}	Roundness, $\delta_{rnd} = r_{rle}/r_e$	
13	δ_{recf}	Rectangular Fit [33]	
14	δ_{den}	Density, $\delta_{den} = A/r_e$	
15	δ_{ellf}	Elliptic Fit [34]	
16	δ_{asp}	Length/Width	
17	L_w	Width (Pxl)	
18	L_l	Length (Pxl)	
19	δ_{asy}	Asymmetry	
20	r_{rle}	Radius of largest enclosed ellipse [35]	

21	r_e	Equivalent radius, $r_e = \sqrt{A/\pi}$	
22	L_{ml}	Length of main line (Pxl)	
23	P	Perimeter	
24	$n_{afr}(Ai)$	Frequency range of area *(Ai~ Ai+250)* (Pxl), *Ai* means the amount of pixels and 250 means the areas increment of 250 pixels of γ' precipitation	
25	dT/dt	Cooling rate(℃/min)	Processing parameter

3 MACHINE LEARNING MODELS

The training of ANN model consists of two parallel processes: a shallow neural network (SNN) training for ranking features, and a deep neural network (DNN) training for predicting the hardness of alloys. The training process of CNN is general. After the CNN model training is completed, real experimental data is used for CNN model validation.

3.1 Microstructural feature weight ranking by a SNN model and DNN training

Because of manual feature engineering, the input data might be excessive due to the reliance of various microstructural descriptors on each other. In order to reduce redundant information, save the training cost of DNN model, and help understanding the importance of each parameter on hardness, a SNN model of single hidden layer, as shown in **Figure 3**(a), is built to calculate the ranking of different descriptors.

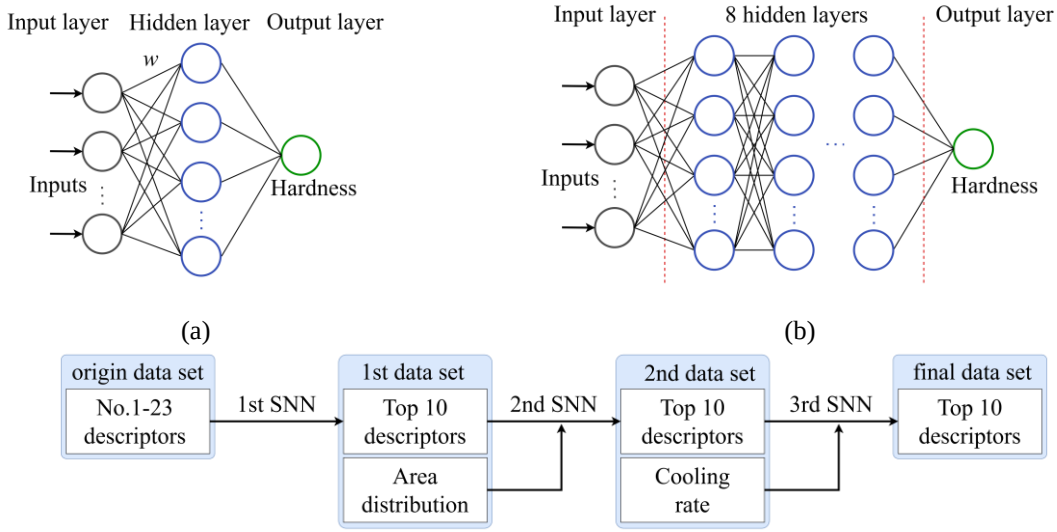

Figure 3. (a) SNN for feature weight ranking, (b) DNN model, (c) three training processes for feature weight ranking.

The training process is performed three times to obtain a more accurate feature weight ranking, which is ultimately used for training the DNN. The data set should reflect the hardness-related characteristics of the alloy as much as possible within the limited features.

The diagram of three training process is shown in **Figure 3**(c). (1) In the 1st training, 23

descriptors (number 1 to 23 in **Table 1**) as input data are used to train the first SNN model. As a result, top 10 types of descriptors can be picked out by the ranking of weighting factors in the first SNN model. (2) In the 2nd training, a new-added parameter referring to area distribution $n_{afr}(Ai)$ together with the above-chosen top 10 parameters consisted input data set to investigate the effect of areas of γ′ precipitates on hardness. (3) In the 3rd training, similarly, cooling rate is added in the top 10 parameters selected from the second training set. Cooling rate is regarded as a remedy of γ′ precipitates internal variable, since it is widely believed to primarily control γ′ precipitates. Since tertiary γ′ precipitates are difficult to be observed except using high-resolution TEM tools, the nano-sized γ′ precipitates are not observed in SEM images and their contributions on the hardness have been missed.

Corresponding to the data sets selected from the three trainings of SNN, three data sets are used to train DNN, and three DNN models are obtained. The DNN is consisted of an input layer, 8 hidden layers and one output layer. The architecture of DNN is shown in **Figure 3**(b).

3.2 Training CNN model and validation with experimental data

Unlike the ANN model used above, CNN has two distinct types of hidden layers: convolutional layers and pooling layers. The CNN model is consisted of one input layer, 4 convolution layers, 4 average pooling layers, 2 full connect layers and one output layer with 2 outputs, as shown in **Figure 4**(a).

The comparisons of test set results between CNN and LBM are shown in **Figure 4**(c). The regression coefficient R^2 of ETCs in x and y direction, as shown in Eq.(1), are very close to 1, which means that this CNN model establishes an accurate relationship between ETCs and the microstructure of RVEs.

$$R^2 = 1 - \frac{\sum_{i=1}^{n}(\mathbf{y}_i - \hat{\mathbf{y}}_i)^2}{\sum_{i=1}^{n}(\mathbf{y}_i - \frac{1}{n}\sum_{i=1}^{n}\mathbf{y}_i)^2} \tag{1}$$

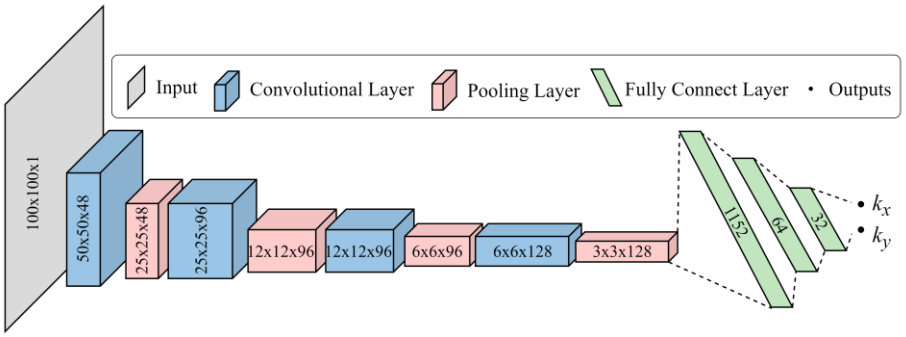

(a)

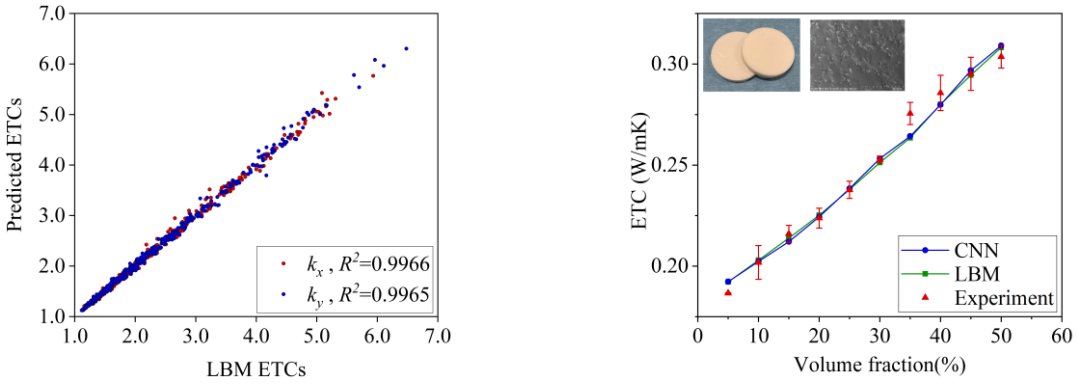

(b) (c)

Figure 4. (a) CNN model architecture, (b) comparisons between CNN and LBM predictions of test set, (c) photo and SEM of PDMS composites, comparisons between LBM, CNN predictions and experiment results of the composites, error bars represent the standard deviation of three parallel tests.

The CNN model is validated by real experimental data. The experimental data is generated involving composite materials with specifically customized volume fractions of inclusions. The PDMS(Polydimethylsiloxane) matrix composite is fabricated and tested. The photos and SEM of some material samples are shown in the **Figure 4**(a). According to SEM and raw material properties, RVEs and corresponding ETCs are generated. The results comparisons between real experimental data, CNN and LBM predictions are shown in **Figure 4**(b). The prediction results of the CNN model are very consistent with the LBM, and the R^2 value is above 0.99. The predictions of LBM and CNN model are both close to that of real experiment, which proves that the data generated by LBM is reliable, and the CNN model can well capture the results of LBM.

4 RESULTS AND DISCUSSIONS

4.1 Comparison of three ANN models

For ANN models predicting hardness of the alloy specimen, the prediction results of test set by 3 SNN and 3 DNN models are shown in **Figure 5**. With the training of three different microstructure descriptors data sets, the R^2 of both SNN and DNN models gradually increased. The 1st SNN and DNN have lower prediction accuracy. This might because they are training by the 23 microstructural descriptors, the training data has too much interference information or the material properties are not fully described.

In the 2nd training, the R^2 of SNN and DNN both improved slightly. This might be ascribed to the role of size distribution rather than the conventional wisdom that have used average precipitate size as the controlling parameter to calculate shearing stress. It is worth mentioning that since the $n_{afr}(10)$ parameter is added to the descriptors set, $n_{afr}(10)$ become the third most important parameter in the 2nd feature ranking, illustrating its importance to hardness. The improvement of R^2 is believed to be closely to the consideration of area distribution descriptor.

In the 3rd training study, cooling rate is added in to descriptors set. It is the most important parameter that controlling hardness according to feature ranking. And the highest R^2 values of 3nd SNN and DNN also demonstrated that prediction accuracy is improved by introducing the

parameter of cooling rate.

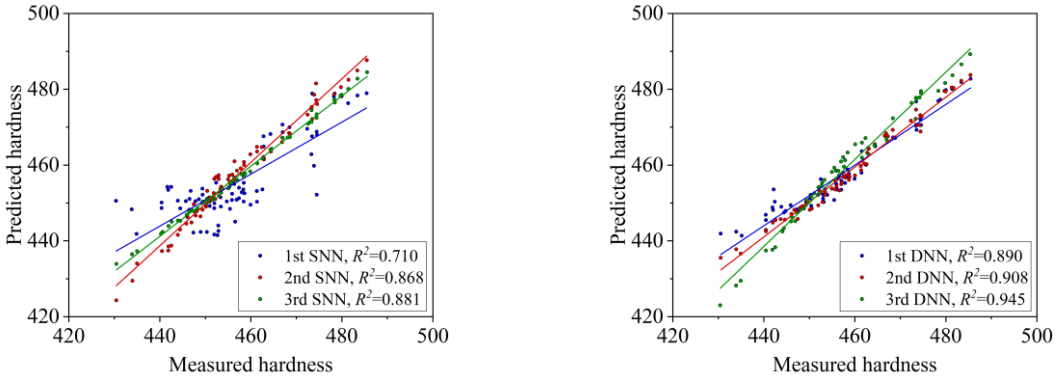

(a) (b)

Figure 5. Hardness results comparison between prediction and experimental measurements, the straight lines represent the linear fit of each model prediction, 3 training results are represented by the blue, red and green dots and linear fit curves respectively, (a) prediction by SNN, (b) prediction by DNN.

4.2 Comparation between ML models and analytical models

The ANN and CNN are also employed to predict samples out of training set. And the comparation between ML model and some traditional models are as shown in **Figure 6**. It can be seen that the accuracy of ML models is higher than traditional analytical models. This indicates that ML models have predictive capabilities exceed physics-based models. ML models can receive more features as inputs and automatically develop reasoning abilities that are different from human logic. On the contrary, the understanding of the mapping between microstructure and macroscopic properties in physics-based models is not comprehensive enough. For example, the Jagjiwanram model[27] cannot take the aspect ratio of fibers of consideration, and the H-S model[28] cannot consider the scale effect of particles.

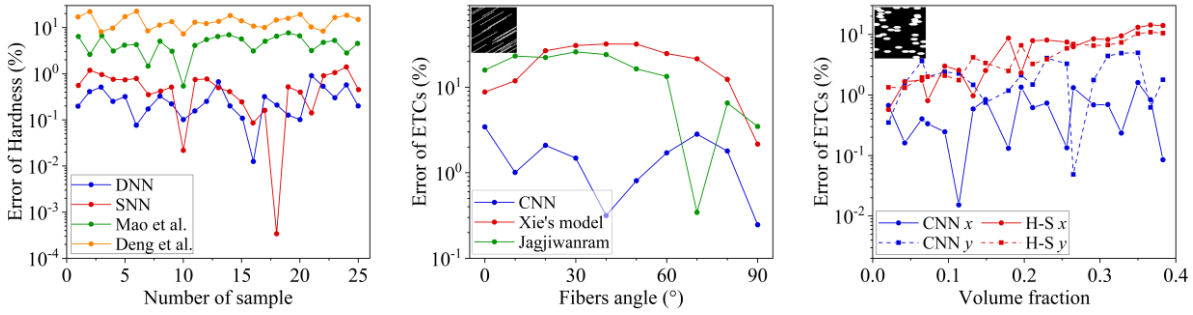

(a) (b) (c)

Figure 6. Error plots of ML models prediction and traditional analytical models, (a) hardness results of DNN, SNN, Mao et al.[29], Deng et al.[30], the experimental measurement is regarded as ground truth, (b) ETCs results of RVEs of fibrous material with parallel fibers by CNN, Xie's model[25], Jagjiwanram model[27], (c) ETCs results of RVE of particulate material with aligned elliptical inclusions by CNN and H-S model[28]. (The LBM result is regarded as ground truth for (b) and (c))

4.3 Prediction for novel microstructures

To further explore the potential of the CNN model, two sets of novel RVEs are generated: 50 hybrid RVEs of fibrous and particulate composites, 10 SEM RVEs from real materials images[31-33]. The hybrid RVE is created by performing matrix addition operations on two models represented in matrix form from QSGS and RGGM methods, respectively. The SEM RVEs are binarized and resized for CNN prediction. Then the ETCs are predicted by both LBM and CNN. **Figure 7** shows the comparison between CNN and LBM predictions. Obviously, the prediction accuracy of CNN for new samples is still very high, with R^2 above 0.99.

Although the CNN is trained using two types of microstructure RVEs, it itself does not differentiate the particulate or fibrous types of microstructures. That is to say, CNN can predict the ETC of any (artificially defined) type of microstructure.

CNN's ability to understand images is implicit, and the weights, bias terms and feature maps in the model do not have clear physical meanings, some feature maps are shown in the **Figure 7**(c). The distinct mapping utilized in this process, as opposed to artificially defined physical models, enables the prediction of macroscopic properties corresponding to any microstructure type.

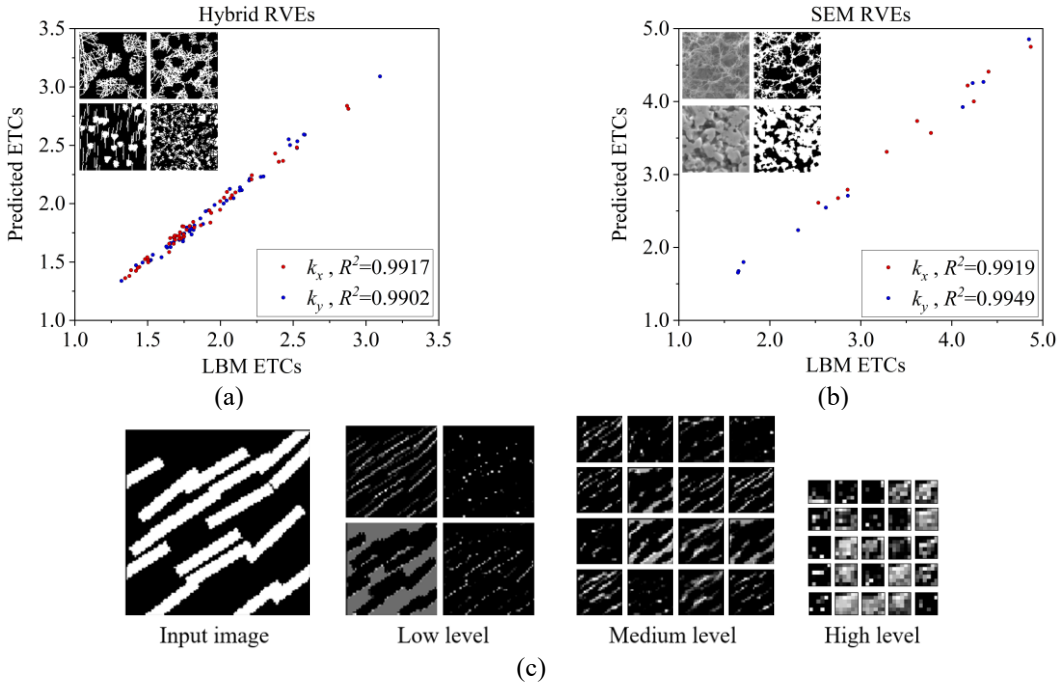

Figure 7. (a) Results of 50 hybrid RVEs by CNN and LBM, (b) results of 10 SEM RVEs, (c) visualization of CNN feature map

5 CONCLUSIONS

This paper presents two kinds of machine learning models to predict macroscopic properties of heterogeneous material by microstructural data. Although the training data and processes of the models are slightly different, both ANN and CNN model's prediction are more accurate and faster than traditional physical models. The following conclusions are drawn:

(1) The ANN model can rank input features by importance. Not only can it eliminate redundant material descriptors (for models that predict the hardness of such alloys), but it can also show the influence of a certain material parameter on the hardness, which is useful for guiding material design process.

(2) The CNN model has advantage of without manual feature engineering, which makes its use more convenient. At the same time, CNN does not "identify" the type of microstructure, but only realizes the perception of microstructure through convolution and pooling layers. So, with sufficient training data, the artificial microstructure classification (particles, fibres, various shapes, etc.) has less impact on the predictive power of the CNN model.

(3) Based on enough and reliable microstructural and macroscopic data for training, ML models can predict macroscopic properties, such as Young's modulus, hardness, etc., that can be correlated to the material's microstructure. This underscores the promising role of machine learning in propelling advancements in materials science and accelerating the creation of materials tailored to meet specific property requirements.

ACKNOWLEDGEMENT

H.F. Zhao acknowledges the support from China Manned Space Engineering Program and the Research Fund of Aero Engine Corporation of China (AECC) through the Grant No. HFZL2022CXY026-2.

REFERENCES

[1] T. W. Clyne and D. Hull, "An Introduction to Composite Materials," 2019, doi: DOI: 10.1017/9781139050586.

[2] J. Tapia-López, M. I. Pech-Canul, and H. M. García, "Processing, microstructure, properties, and applications of MoSi2-containing composites: a review," *Frontiers in Materials*, vol. 10, 2023, doi: 10.3389/fmats.2023.1165245.

[3] J. Li, Q. Zhang, R. Huang, X. Li, and H. Gao, "Towards understanding the structure–property relationships of heterogeneous-structured materials," *Scripta Materialia*, vol. 186, pp. 304-311, 2020, doi: 10.1016/j.scriptamat.2020.05.013.

[4] Q. Shao *et al.*, "Material Twin for composite material microstructure generation and reconstruction," *Composites Part C: Open Access*, vol. 7, p. 100216, 2022/03/01/ 2022, doi: https://doi.org/10.1016/j.jcomc.2021.100216.

[5] S. Swadesh Kumar *et al.*, "Understanding Composites and Intermetallic: Microstructure, Properties, and Applications," *E3S Web of Conferences*, vol. 430, 2023, doi: 10.1051/e3sconf/202343001196.

[6] R. Hill, "A self-consistent mechanics of composite materials," *Journal of the Mechanics and Physics of Solids*, vol. 13, no. 4, pp. 213-222, 1965/08/01/ 1965, doi: https://doi.org/10.1016/0022-5096(65)90010-4.

[7] T. A. Mori and K. Tanaka, "Average stress in matrix and average elastic energy of materials with misfitting inclusions," *Acta Metallurgica*, vol. 21, pp. 571-574, 1973.

[8] S. Torquato and H. W. Haslach Jr, "Random heterogeneous materials: microstructure and macroscopic properties," *Appl. Mech. Rev.*, vol. 55, no. 4, pp. B62-B63, 2002.

[9] J. Wei *et al.*, "Machine learning in materials science," *InfoMat*, vol. 1, no. 3, pp. 338-358, 2019, doi: https://doi.org/10.1002/inf2.12028.
[10] J. F. Rodrigues, Jr., L. Florea, M. C. F. de Oliveira, D. Diamond, and O. N. Oliveira, Jr., "Big data and machine learning for materials science," *Discov Mater*, vol. 1, no. 1, p. 12, 2021, doi: 10.1007/s43939-021-00012-0.
[11] C. Wang, H. Fu, L. Jiang, D. Xue, and J. Xie, "A property-oriented design strategy for high performance copper alloys via machine learning," *npj Computational Materials*, vol. 5, no. 1, 2019, doi: 10.1038/s41524-019-0227-7.
[12] Z. Pei *et al.*, "Machine‐Learning Microstructure for Inverse Material Design," *Advanced Science*, vol. 8, no. 23, 2021, doi: 10.1002/advs.202101207.
[13] L. B. Tan and N. D. P. Nhat, "Prediction and Optimization of Process Parameters for Composite Thermoforming Using a Machine Learning Approach," *Polymers (Basel)*, vol. 14, no. 14, Jul 12 2022, doi: 10.3390/polym14142838.
[14] R. Liu, A. Kumar, Z. Chen, A. Agrawal, V. Sundararaghavan, and A. Choudhary, "A predictive machine learning approach for microstructure optimization and materials design," *Scientific Reports*, vol. 5, no. 1, 2015, doi: 10.1038/srep11551.
[15] K. Guo, Z. Yang, C. H. Yu, and M. J. Buehler, "Artificial intelligence and machine learning in design of mechanical materials," *Mater Horiz*, vol. 8, no. 4, pp. 1153-1172, Apr 1 2021, doi: 10.1039/d0mh01451f.
[16] Y. Liu, T. Zhao, W. Ju, and S. Shi, "Materials discovery and design using machine learning," *Journal of Materiomics*, vol. 3, no. 3, pp. 159-177, 2017, doi: 10.1016/j.jmat.2017.08.002.
[17] S. P. Ong, "Accelerating materials science with high-throughput computations and machine learning," *Computational Materials Science*, vol. 161, pp. 143-150, 2019, doi: 10.1016/j.commatsci.2019.01.013.
[18] I. D. Jung *et al.*, "Artificial intelligence for the prediction of tensile properties by using microstructural parameters in high strength steels," *Materialia*, vol. 11, 2020, doi: 10.1016/j.mtla.2020.100699.
[19] K. Kim *et al.*, "A machine learning approach for predicting heat transfer characteristics in micro-pin fin heat sinks," *International Journal of Heat and Mass Transfer*, vol. 194, 2022, doi: 10.1016/j.ijheatmasstransfer.2022.123087.
[20] A. Beniwal, R. Dadhich, and A. Alankar, "Deep learning based predictive modeling for structure-property linkages," *Materialia*, vol. 8, 2019, doi: 10.1016/j.mtla.2019.100435.
[21] K. M. Graczyk and M. Matyka, "Predicting porosity, permeability, and tortuosity of porous media from images by deep learning," *Sci Rep*, vol. 10, no. 1, p. 21488, Dec 8 2020, doi: 10.1038/s41598-020-78415-x.
[22] Y. Li *et al.*, "Neural network model for correlating microstructural features and hardness properties of nickel-based superalloys," *Journal of Materials Research and Technology*, vol. 9, no. 6, pp. 14467-14477, 2020, doi: 10.1016/j.jmrt.2020.10.042.
[23] C. Shen, Q. Sheng, and H. Zhao, "Predicting effective thermal conductivity of fibrous and particulate composite materials using convolutional neural network," *Mechanics of Materials*, vol. 186, 2023, doi: 10.1016/j.mechmat.2023.104804.
[24] M. Wang, J. Wang, N. Pan, and S. Chen, "Mesoscopic predictions of the effective thermal conductivity for microscale random porous media," *Phys Rev E Stat Nonlin Soft*

Matter Phys, vol. 75, no. 3 Pt 2, p. 036702, Mar 2007, doi: 10.1103/PhysRevE.75.036702.

[25] T. Xie and Y.-L. He, "Heat transfer characteristics of silica aerogel composite materials: Structure reconstruction and numerical modeling," *International Journal of Heat and Mass Transfer*, vol. 95, pp. 621-635, 2016, doi: 10.1016/j.ijheatmasstransfer.2015.12.025.

[26] A. Mohamad, *Lattice Boltzmann Method: Fundamentals and Engineering Applications with Computer Codes*. Springer, 2019.

[27] Jagjiwanram and R. Singh, "Effective thermal conductivity of highly porous two-phase systems," *Applied Thermal Engineering*, vol. 24, no. 17-18, pp. 2727-2735, 2004, doi: 10.1016/j.applthermaleng.2004.03.010.

[28] Z. Hashin and S. Shtrikman, "A variational approach to the theory of the elastic behaviour of multiphase materials," *Journal of the Mechanics and Physics of Solids*, vol. 11, no. 2, pp. 127-140, 1963/03/01/ 1963, doi: https://doi.org/10.1016/0022-5096(63)90060-7.

[29] J. Mao, K.-M. Chang, W. Yang, D. U. Furrer, K. Ray, and S. P. Vaze, "Cooling precipitation and strengthening study in powder metallurgy superalloy Rene88DT," *Materials Science and Engineering: A*, vol. 332, no. 1, pp. 318-329, 2002/07/01/ 2002, doi: https://doi.org/10.1016/S0921-5093(01)01758-0.

[30] W. Deng, D. Zhang, H. Wu, Z. Huang, K. Zhou, and L. Jiang, "Prediction of yield strength in a polycrystalline nickel base superalloy during interrupt cooling," *Scripta Materialia*, vol. 183, pp. 139-143, 2020/07/01/ 2020, doi: https://doi.org/10.1016/j.scriptamat.2020.03.034.

[31] J.-F. Justin, A. Julian-Jankowiak, V. Guérineau, V. Mathivet, and A. Debarre, "Ultra-high temperature ceramics developments for hypersonic applications," *CEAS Aeronautical Journal*, vol. 11, no. 3, pp. 651-664, 2020/09/01 2020, doi: 10.1007/s13272-020-00445-y.

[32] N. M. Larson and F. W. Zok, "In-situ 3D visualization of composite microstructure during polymer-to-ceramic conversion," *Acta Materialia*, vol. 144, pp. 579-589, 2018, doi: 10.1016/j.actamat.2017.10.054.

[33] Z. Qian *et al.*, "Superelastic and ultralight polyimide aerogels as thermal insulators and particulate air filters," *Journal of Materials Chemistry A*, vol. 6, no. 3, pp. 828-832, 2018, doi: 10.1039/c7ta09054d.